The Plant Cell, Vol. 20: 1665–1677, June 2008, www.plantcell.org © 2008 American Society of Plant Biologists

Channelrhodopsin-1 Initiates Phototaxis and Photophobic Responses in *Chlamydomonas* by Immediate Light-Induced Depolarization [W]

Peter Berthold,[a] Satoshi P. Tsunoda,[a] Oliver P. Ernst,[b] Wolfgang Mages,[c] Dietrich Gradmann,[d] and Peter Hegemann[a,1]

[a] Institute for Biology, Experimental Biophysics, Humboldt-Universität, 10115 Berlin, Germany
[b] Institute for Medical Physics and Biophysics, Charité-Universitätsmedizin Berlin, 10117 Berlin, Germany
[c] Institute for Genetics, Universität Regensburg, 93040 Regensburg, Germany
[d] A.-v.-Haller-Institut der Universität, 37073 Göttingen, Germany

Channelrhodopsins (CHR1 and CHR2) are light-gated ion channels acting as sensory photoreceptors in *Chlamydomonas reinhardtii*. In neuroscience, they are used to trigger action potentials by light in neuronal cells, tissues, or living animals. Here, we demonstrate that *Chlamydomonas* cells with low CHR2 content exhibit photophobic and phototactic responses that strictly depend on the availability of CHR1. Since CHR1 was described as a H^+-channel, the ion specificity of CHR1 was reinvestigated in *Xenopus laevis* oocytes. Our experiments show that, in addition to H^+, CHR1 also conducts Na^+, K^+, and Ca^{2+}. The kinetic selectivity analysis demonstrates that H^+ selectivity is not due to specific translocation but due to selective ion binding. Purified recombinant CHR1 consists of two isoforms with different absorption maxima, $CHR1_{505}$ and $CHR1_{463}$, that are in pH-dependent equilibrium. Thus, CHR1 is a photochromic and protochromic sensory photoreceptor that functions as a light-activated cation channel mediating phototactic and photophobic responses via depolarizing currents in a wide range of ionic conditions.

INTRODUCTION

Rhodopsins are membrane-spanning proteins (opsins) with a covalently bound retinal serving as the chromophore. Three rhodopsin classes are distinguished by their different functions: (1) sensory rhodopsins operate via an enzymatic signaling system as visual photoreceptors in animal eyes or sensors for phototaxis in prokaryotes; (2) light-driven ion pumps for H^+ and Cl^- form a primordial mechanism for photosynthetic energy conversion in archaea and eubacteria (Sharma et al., 2006); and (3) channelrhodopsins mediate light-induced conductance of H^+ and other cations in algal eyes (Hegemann, 2008). Even more functions are expected to exist for rhodopsins, considering the large number of genetically identified rhodopsins for which no physiological function has yet been assigned. For instance, the unicellular alga *Chlamydomonas reinhardtii* contains at least seven rhodopsin-related proteins (Hegemann et al., 2001), but only the two channelrhodopsins CHR1 ($\lambda_{max} = 500$ nm) and CHR2 ($\lambda_{max} = 470$ nm) have been functionally characterized in some detail. CHRs are microbial-type rhodopsins with intrinsic, light-gated ion conductance. CHR1 has been reported to be selective for H^+, whereas CHR2 was shown to conduct Na^+, K^+, and Ca^{2+} (Nagel et al., 2002, 2003). Channelrhodopsins have been used to generate action potentials in normally light-insensitive mammalian cells (Boyden et al., 2005; Li et al., 2005; Nagel et al., 2005; Bi et al., 2006; Ishizuka et al., 2006; Schroll et al., 2006; Zhang et al., 2006; Zhang and Oertner, 2007). These light-induced action potentials can be triggered with unprecedented spatio-temporal precision in cultured cells and tissues. For the sake of applying channelrhodopsins as a neuroanalytical tool, a deeper understanding of the kinetics and ion specificities of these proteins is of great interest.

CHRs are thought to be the photoreceptors that, in vivo, mediate the photoreceptor current I_P in the eye of *Chlamydomonas* and related algae (Litvin et al., 1978; Harz and Hegemann, 1991; Holland et al., 1996; Ehlenbeck et al., 2002). The photoreceptor current triggers phototactic and photophobic responses. The photophobic response comprises backward swimming for half a second upon sudden changes in light intensity, whereas phototaxis is the sum of biased directional changes that appear as smooth swimming toward or away from a light source at high light intensities (Hegemann and Bruck, 1989). Photoreceptor currents are carried by Ca^{2+} and H^+ or by K^+ or Na^+ when the ion concentration in the medium is high enough (Nonnengasser et al., 1996; Ehlenbeck et al., 2002). Action spectra for electrical responses are rhodopsin shaped and show maxima between 495 and 505 nm in the strains CW2 or 495+ (Harz and Hegemann, 1991; Sineshchekov et al., 1994; Ehlenbeck et al., 2002). The action spectra for electrical responses match the low intensity action spectra for phototaxis and photophobic responses, which all peak at 495 to 505 nm (Foster et al., 1984; Hegemann and Uhl, 1990).

The close correlation between the action spectra for the *Chlamydomonas* photoreceptor current and behavioral responses with the action spectrum of CHR1 photocurrents in

[1] Address correspondence to hegemann@rz.hu-berlin.de.
The author responsible for distribution of materials integral to the findings presented in this article in accordance with the policy described in the Instructions for Authors (www.plantcell.org) is: Peter Hegemann (hegemann@rz.hu-berlin.de).
[W] Online version contains Web-only data.
www.plantcell.org/cgi/doi/10.1105/tpc.108.057919

Xenopus laevis oocytes (λ_{max} = 500 nm; Nagel et al., 2002) suggested that CHR1 is the dominant photoreceptor for both phototaxis and photophobic responses. However, high intensity spectra show a shoulder near 470 nm (Nultsch et al., 1971). Using a CHR1-RNA interference (RNAi) transformant with low amounts of CHR1, Sineshchekov et al. (2002) attempted to functionally connect channelrhodopsins and phototaxis. In these transformants, the photoreceptor current was reduced, which provided strong experimental evidence that CHR1 operated as the responsible photoreceptor. However, the relative contributions of CHR1 and CHR2 remained unresolved. Interestingly, the action spectrum of the CHR1-RNAi transformant for photoreceptor currents is blue shifted, and this shift was assigned to a contribution of CHR2 (λ_{max} = 470 nm) activity (Sineshchekov et al., 2002). This interpretation is supported, first, by the action spectrum of CHR2 in *Xenopus* oocytes (Nagel et al., 2002) and, second, by the absorption spectra of purified CHR2 from *Chlamydomonas* and the close relative *Volvox carteri*, which all show maxima around 470 nm (Bamann et al., 2008; Ernst et al., 2008). The CHR1-RNAi transformant further showed slower and delayed photocurrents after flash activation. It was suggested that CHR2 initiates the delayed currents (Sineshchekov et al., 2002) and that the photocurrent is generated by a secondary channel that is regulated via a diffusible messenger, analogous to the signal-transducing process in animal vision (reviewed in Spudich 2006; Jung, 2007; Hegemann 2008). Govorunova et al. (2004) analyzed a new antisense transformant with defined CHR1 and CHR2 content using computerized motion analysis and demonstrated that both CHR1 and CHR2 can serve as photoreceptors for phobic responses.

Since CHR1 is assumed to conduct H^+ only, it was argued that it would hardly carry the photoreceptor current at neutral or alkaline pH, which made involvement of a secondary cation channel for membrane depolarization a likely option (Kateriya et al., 2004; Sineshchekov and Spudich, 2005). However, in the eyespot proteome, in which CHR1 and CHR2 appear as abundant proteins, no protein with homology to traditional cation channels appeared with significant representation (Schmidt et al., 2006).

The first aim of this study was therefore to test whether CHR1 can cause electric depolarization of the cell membrane by itself conducting a light-induced, unselective current. In this context, the cation selectivity of CHR1 is crucial. Since H^+ selectivity has been stated for CHR1 (Nagel et al., 2002), in contrast with CHR2, which conducts Na^+, K^+, and Ca^{2+} as well (Nagel et al., 2003), the second aim of this study was to investigate cation selectivity of CHR1 more rigorously. For this purpose, we applied a kinetic selectivity analysis, in which the steady state current–voltage relationships (*I*/*E*-curves) of an enzyme kinetic reaction scheme for competitive translocation of alternate substrates were fitted to experimental *I*/*E*-curves obtained under various ionic conditions. We found that the relative selectivity of CHR1 for H^+ compared with alternate cations can be assigned to binding selectivity, whereas translocation of ions appears virtually unselective. Finally, we show that CHR1 is a photochromic and protochromic protein with two pH-dependent isoforms differing in their maximal absorption by ~40 nm. The absorption of both isoforms may contribute to the action spectra for phototaxis and photophobic responses at low and high light intensities. The results support the idea that, under most environmental conditions, CHR1 mediates light-induced depolarization in *Chlamydomonas*, which serves as an early step in signal transduction from the eye to the flagella of green algae.

RESULTS

Protein Quantification

Since nearly all electrophysiological studies on single *Chlamydomonas* cells have been conducted on the cell wall–deficient strain CW2 (Harz and Hegemann, 1991; Nonnengasser et al., 1996; Ehlenbeck et al., 2002), we measured the content of CHR1 and CHR2 in this strain. Antisera against the C-terminal fragments $CHR1_{310-547}$ or $CHR2_{272-520}$ recognized the authentic protein and weakly cross-reacted with the homologous protein (see Supplemental Figure 1A online). In protein blots of CW2 extracts, CHR1 was recognized under our modified conditions as a protein with apparent molecular mass of 68 kD_{app} and CHR2 as a doublet of ~64 and 66 kD_{app} (Figure 1A; see Supplemental Figure 1B online). Whereas CHR1 migrated faster than CHR2 during PAGE of earlier studies (Sineshchekov et al., 2002; Nagel et al., 2003; Govorunova et al., 2004), our technique, in which cells were directly solubilized in sample buffer, rendered CHR1 as being larger than CHR2. Under nonreducing conditions, CHR1 appeared as a broad band of 140 kD_{app}, indicating that, unlike CHR2, CHR1 forms a covalently linked homo- or heterodimer (see Supplemental Figure 1B online). Differentiation of CW2 cells under nitrogen deficiency into sexually competent gametes led to a twofold increase of CHR1, whereas CHR2 was reduced in its concentration from almost 40% to below 5% of total CHR protein (Figure 1A; see Supplemental Figure 1C online), which is in contrast with strain 495(+) where the CHR2/CHR1 ratio increased during gametogenesis (Govorunova et al., 2004). The sum of CHR1 and CHR2 in CW2 was determined by comparing the immunoresponse of a defined number of cells on the gel with that of a defined amount of recombinant protein fragment. The sum is in the range of 120,000 molecules per gametic cell, which is four times higher than our earlier estimates based on retinal extraction (Beckmann and Hegemann, 1991) and close to the values determined for strain 495 by Govorunova et al. (2004).

Processing of CHR1 RNA and Generation of Antisense Strains

We generated CHR1 antisense strains by transforming CW2 cells with a plasmid containing a forward genomic CHR1-encoding fragment (also named the *CHLAMYOPSIN3* [*COP3*] fragment according to the gene name) and a reverse complementary cDNA (Figure 1B) under the transcriptional control of a *HSP70*/*RBCS2* promoter hybrid (AR-promoter) (Schroda et al., 2000). After sequencing the genomic DNA, we found that during RNA processing, one C-nucleotide was inserted at the end of exon 4 at position 504 bp of the cDNA. This C-nucleotide was absent in the genomic DNA of all strains we tested (CC124 [wild type], CW2, CW15, and CW92) but present in the *COP3*-cDNA clone

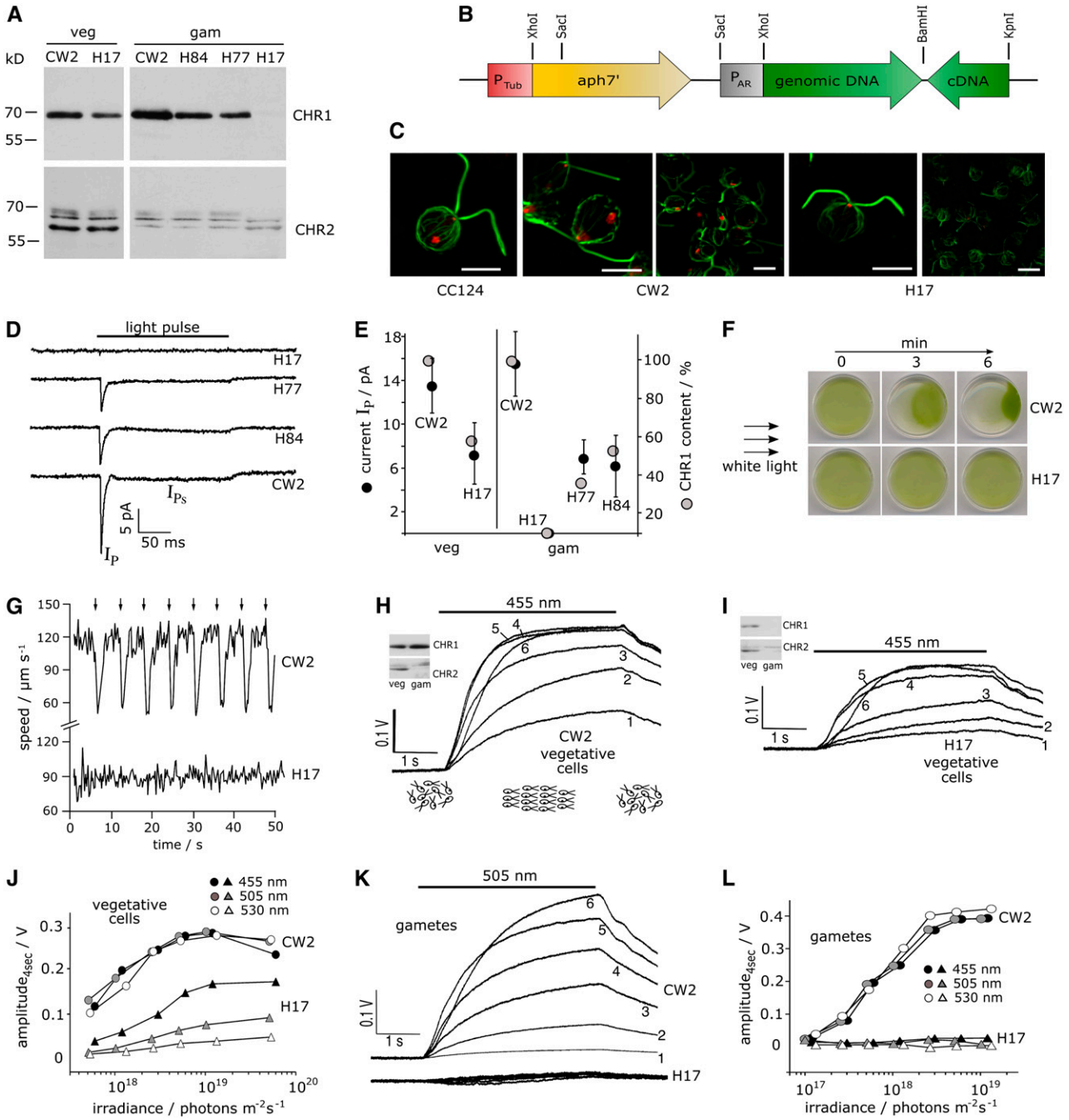

Figure 1. Downregulation of ChR1 in the *Chlamydomonas* Strain CW2.

(A) A representative immunoblot analysis of three RNAi mutants, H17, H77, and H84, and of the untransformed CW2 recipient strain ($n = 3$). Vegetative cells (veg) and gametes (gam) were analyzed with anti-CHR1 antibody or anti-CHR2 antibody.

(B) Schematic of the pPB-ASCHR1 plasmid used for *Chlamydomonas* transformation, containing the hygromycin selection marker (aph7′) (Berthold et al., 2002) driven by the *Chlamydomonas* β-tubulin promotor (P_{Tub}) and the RNAi hairpin construct (*COP3* genomic DNA, 1538 to 3190 bp, and cDNA, 471 to 972 bp in antisense direction) under control of the Hsp79/RbcS2-promotor (P_{AR}).

(C) Immunofluorescence of vegetative cells of the wild-type strain CC124 and gametes of CW2 and the RNAi-mutant H17. CHR1 protein is visualized in red, and α-tubulin is shown in green. Bars = 10 µm.

(D) Photoreceptor currents measured from gametes of the recipient strain CW2 and the CHR1 antisense transformants H84, H77, and H17 under the ''eyespot in'' configuration. Cells were stimulated with a green light pulse ($\lambda = 510 \pm 20$ nm, $3 \cdot 10^{22}$ photons $m^{-2}s^{-1}$). I_p and I_{ps} are the fast and slow photoreceptor currents, respectively.

of the EST library (Kazusa DNA Research Institute, Japan) and in *COP3* cDNA that we had amplified three times independently from CW2 cells (see Supplemental Figure 2 online). Such an insertion of a single base pair during RNA processing is rare. It has been reported in the flagellate *Trypanosoma brucei* (Simpson et al., 2004) and in slime mold (*Physarum polycephalum*; Mahendran et al., 1991). This insertion is essential for the translation of full-length CHR1 because without it truncated proteins of 173 (after excision of intron 5) or 263 (without excision of intron 4) amino acids would result. These hypothetical proteins, however, were not detected on protein blots using a peptide antibody against the loop connecting transmembrane helices 1 and 2 of CHR1.

In the *Chlamydomonas* antisense transformants, the amount of CHR1 was quite variable (Figure 1A). Strain H17 expressed 10 to 50% of wild-type CHR1 levels under vegetative conditions (40% in the case of Figure 1A), but CHR1 was almost completely absent in gametes (<1%), suggesting that transcription of the antisense construct is enhanced by nitrogen deficiency. We also noticed that the CHR2 content was only slightly affected in the CHR1 antisense transformants and was reduced during gametogenesis in a similar way as in the wild type. In gametes of the recipient strain CW2, the anti-CHR1 antiserum identified an ~1-μm spot at a position where the eyespot is seen in living cells (Figure 1C), confirming earlier localization of CHR1 (Suzuki et al., 2003). This staining is absent in H17 gametes, confirming the localization of CHR1. The fluorescence at the base of the flagella remained unchanged in strain H17 and was considered nonspecific.

The Photoreceptor Current Is Proportional to the CHR1 Content

Photoreceptor currents were recorded from individual gametes of four antisense transformants under ''eyespot in'' conditions. For this purpose, the eye was sucked into the patch pipette, whereas most of the cell body including the flagella was kept outside. Under these conditions, up to 50% of the total photoreceptor current is monitored, whereas subsequent flagellar currents can hardly be detected (Ehlenbeck et al., 2002). The transient wild-type photoreceptor current I_P reaches a total of 40 pA at high flash intensities. Photocurrents of CHR1 antisense transformants (identical cultures as used for the protein blot in Figure 1A) were smaller (Figure 1D) and, within experimental errors, the peak amplitude corresponded to the amount of CHR1 in each transformant (Figure 1E). No photocurrent could be recorded from CHR1-deficient H17 gametes up to flashes of 10^{22} photons m^{-2} ($\lambda_{max} = 500$ nm), but photocurrents were still visible in H84 and H77 gametes and vegetative H17 cells, which contained 55, 35, and 60% the amount of CHR1 found in the wild type, respectively (Figures 1D and 1E).

CHR1 Mediates Phototaxis and Photophobic Responses

In a first survey, phototaxis was tested in the classical dish test, in which CW2 cells move away from white light with a phototactic velocity of ~100 μm s^{-1} (Foster et al., 1984; Hegemann et al., 1988). In this assay, H17 cells were completely unresponsive (Figure 1F). For more detailed behavioral studies, the swimming speed of the cells must be determined by motion analysis, because transformation of *Chlamydomonas* frequently causes reduction or complete and permanent loss of flagellar beating. For that purpose, individual gametes were tracked microscopically. The swimming speed of H17 cells was 90 μm s^{-1} compared with 120 μm s^{-1} for cells of the CW2 recipient strain (Figure 1G, which is representative of three independent experiments). Repetitive flashing of CW2 cells leads to photophobic responses, seen as sudden and transient reduction of the swimming speed (Hegemann and Bruck, 1989). Such a response was completely absent in H17 gametes, thus supporting earlier findings of Govorunova et al. (2004). Next, phototaxis of cell populations was analyzed by a light scattering assay. Phototaxis of vegetative H17 cells that contained wild-type levels of CHR2 and ~15% of wild-type levels of CHR1 showed good phototaxis in 455-nm light (Figure 1H and 1I, inset). Note that at high light intensities phototaxis was delayed due to an increased

Figure 1. (continued).

(E) Relation between CHR1 content and average I_p amplitude in CW2 and antisense transformants. CHR1 content of CW2 gametes was set at 100%. Protein content and currents were determined from the same culture. Each current amplitude represents an average of five measurements from nine individual cells including SE.

(F) Phototaxis (dish test) of CW2 and H17 gametes. Cells were exposed to white light (~7 W/m^2), and cell migration was observed for 6 min.

(G) Swimming speed of CW2 and H17 gametes and photophobic responses to flashes of green light (arrows; 10 μs, $\lambda = 510 \pm 40$ nm at $3 \cdot 10^{22}$ photons $m^{-2}s^{-1}$).

(H) and **(I)** Phototactic orientation of CW2 **(H)** and H17 **(I)** vegetative parallel cultures as monitored in a light scattering apparatus during light pulses of 455 ± 20 nm at six different light intensities, numbered 1 to 6 ($6.0 \cdot 10^{17}$, $1.2 \cdot 10^{18}$, $2.4 \cdot 10^{18}$, $6.0 \cdot 10^{18}$, $1.2 \cdot 10^{19}$, and $6.0 \cdot 10^{19}$ photons $m^{-2}s^{-1}$, respectively). The traces are averages of three individual measurements from one out of two similar independent experiments. The CHR1 and CHR2 content at the time of the measurement may be estimated from the protein blots (insets). The drawing at the bottom explains the orientation pattern of the culture during the experiment.

(J) The signal amplitudes of CW2 and H17 vegetative cells after 4 s of exposure to three characteristic wavelengths of light (455, 505, and 530 ± 20 nm) plotted versus the photon irradiance.

(K) Phototactic orientation of CW2 and H17 gametes (parallel cultures) as monitored in a light scattering apparatus during light pulses of 505 ± 20 nm and at different light intensities.

(L) The signal amplitudes measured in CW2 and H17 gametes after 4 s in the light plotted against the photon irradiance.

adaptation period (trace 6). The phototactic rate of H17 was reduced by 30% due to slower swimming (90 $\mu m\ s^{-1}$ versus 120 $\mu m\ s^{-1}$ in the wild type), but the sensitivity was only twofold below that of the wild type (Figures 1H and 1I), demonstrating that the signal transduction system from the eye to the flagellum was functional. Vegetative H17 cells, however, showed weak responses to 505- and 530-nm light (Figure 1J). Even clearer was the result with gametes (Figure 1K). The dominant lower CHR2 band was lost during gametogenesis in both cultures, CW2 and H17, whereas CHR1 disappeared in H17 only (Figures 1H and 1I, insets). Phototaxis in wild-type gametes improved relative to vegetative cells because unlike unsynchronized vegetative cells, gametic cells are all motile (Figure 1K). By contrast, phototaxis of H17 gametes was completely lost, independent of the wavelength used for stimulation (Figures 1K and 1L).

Photoresponses at pH 9

Since we had established that CHR1 is the dominant photoreceptor for phototaxis in CW2 gametes, the question that arose was how a light-gated H^+-channel can mediate photocurrents, especially at alkaline pH_o. To address this question, we reanalyzed the *Chlamydomonas* photocurrents at pH_o 9 (510 nm; Figure 2A). In CW2 gametes, the currents were ~30% smaller but kinetically similar to those reported over the years for pH 6.0 or 7 (Ehlenbeck et al., 2002). The situation was a little different for photo-orientation of the cells upon step-up stimulation (Figure 2B). At pH_o 9, the photophobic response to 510-nm light was reduced compared with pH 6.8, with the consequence that the cells orientated themselves away from the light without delay. The phototactic velocity was also slightly reduced, but all cells were reactive as seen from the final amplitude. After several seconds, phototaxis at pH_o 6.8 declined due to light adaptation, whereas at pH_o 9, phototaxis remained quite stable. In H17 gametes, the response to 510-nm flashes was totally absent, confirming that, also at alkaline pH, photomovement in CW2 gametes is under the control of CHR1.

CHR1 Conducts H^+ and the Physiologically Relevant Cations Na^+, K^+, and Ca^{2+}

To address the question of how a light-gated proton channel controls orientation of the cells in the light at high pH, we reinvestigated the photoreceptor current of CHR1 in *Xenopus* oocytes, focusing on the ion specificity. Photocurrents were recorded at extracellular pH values (pH_o) between pH_o 4 and pH_o 9. As reported in our earlier study (Nagel et al., 2002), photocurrents were large at acidic conditions and small at high pH_o, but they were not proportional to the external H^+ concentration, even at high negative voltage. Representative examples of photocurrents recorded at pH_o 6 and 9 are shown in Figures 3A and 3B, respectively. At pH_o 6 and −125 mV, photocurrents were 15 to 20% larger in the presence of 100 mM Na^+ or Li^+ compared with photocurrents in the presence of 100 mM *N*-methyl-glucamine (NMG^+) (Figures 3A and 3C). Since NMG is not conducted by cation channels (Hille, 2001), we consider currents recorded in the presence of 100 mM NMG as pure H^+ currents. At pH_o 7.5, photocurrents in NMG are approximately eightfold less than those at pH_o 6, but the difference between pure H^+ influx and total Na^+ influx at 100 mM NaCl remained quite similar (Figure 3C). At pH_o 7.5, but not at pH_o 6, external K^+ increased the current at negative voltage, suggesting that K^+ is also conducted but competes with H^+ to some extent. At pH_o 9, the H^+ currents were virtually absent, but cationic currents were still recorded (Figures 3B and 3C). The reversal potential shifted with increasing extracellular ions to more positive voltages, as exemplified for

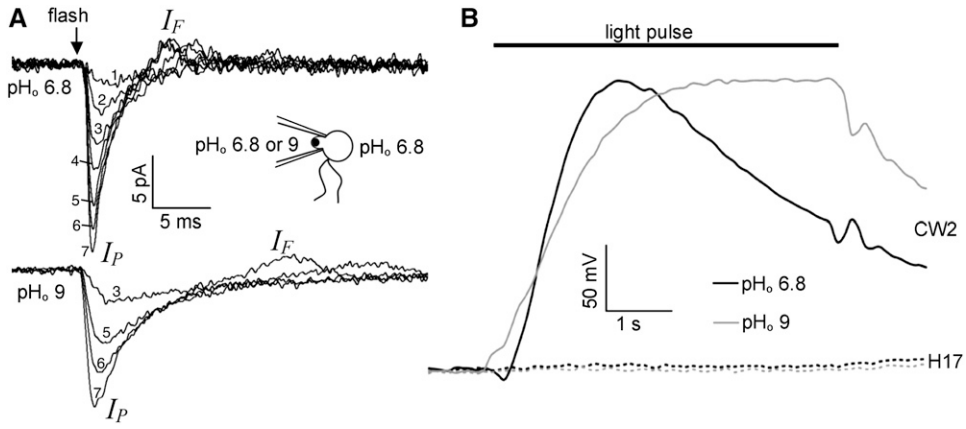

Figure 2. Photocurrents and Phototaxis at pH_o 9.

(A) Flash-induced photocurrent I_P and the subsequent flagellar current I_F of CW2 gametes at pH_o 6.8 and 9 in the "eyespot in" configuration. Cells were stimulated with flashes of 510 ± 40 nm for a 10-μs duration (1, 1%; 2, 2.5%; 3, 6%; 4, 10%; 5, 25%; 6, 50%; 7, 100%, corresponding to $2.2 \cdot 10^{19}$ photons/m^2). pH_o in the bath solution was kept at 6.8 as indicated in the diagram.

(B) Initial phototactic activity of CW2 and H17 gametes at pH_o 6.8 and 9 upon stimulation with a short light pulse of 510 ± 20 nm ($1 \cdot 10^{18}$ photons $m^{-2}\ s^{-1}$). A signal of 100 $mV \cdot s^{-1}$ corresponds to a phototactic movement of ~100 $\mu m\ s^{-1}$. Note that this assay only allows reliable recording of the cell movement during a few seconds after the light is switched on (Uhl and Hegemann, 1990).

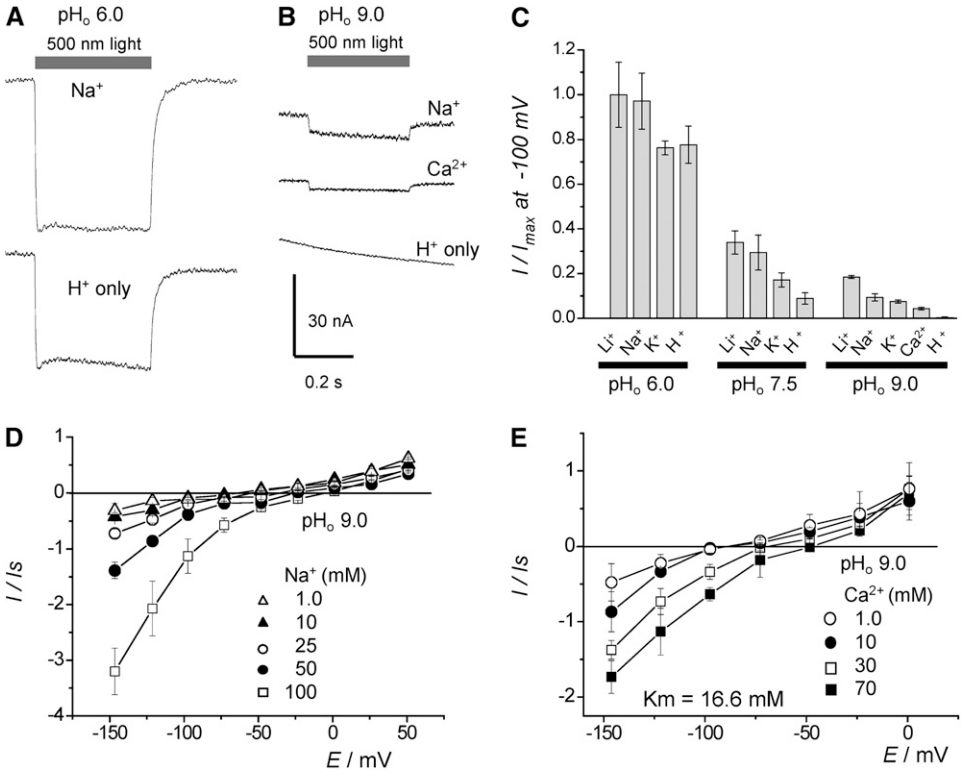

Figure 3. Cation Dependence of the CHR1 Photocurrents.

CHR1 was expressed in *Xenopus* oocytes to measure light-induced currents, using the two-electrode voltage-clamp technique.

(A) Photocurrents recorded at pH$_o$ 6.0. Inward photocurrents were observed upon illumination ($\lambda = 500 \pm 40$ nm, shown as a bar) in the presence (top) and absence (bottom) of 100 mM Na^+ in the bath solution. The membrane potential was held at –125 mV. The traces shown are recorded from the same oocytes ($n = 6$).

(B) Photocurrents recorded at pH$_o$ 9.0. In the presence of 100 mM Na^+ in the bath solution (top), inward currents were observed upon illumination, whereas almost no current was observed in the absence of Na^+ (bottom). Currents were also observed when Na^+ was exchanged for 70 mM Ca^{2+} (middle). The traces shown are recorded from the same oocyte ($n = 5$). Experiments were performed at pH$_o$ 9.0, where H^+ inward currents are negligible. The membrane potential was held at –125 mV.

(C) Current ratios for different cations. Inward photocurrents at –100 mV were normalized to those measured at 100 mM Na^+, pH$_o$ 6. Photocurrents were larger at lower pHo due to the contribution of H^+ permeation. Net H^+ permeation is estimated from the measurement with 100 mM NMG-Cl. Note that significant Ca^{2+} conductance was observed at pH$_o$ 9.0.

(D) [Na^+] dependence of the CHR1 photocurrent. *I/V* plot of the photocurrent at different [Na^+]. Bath solution contained 0.1 mM $CaCl_2$, 0.1 mM $MgCl_2$, 5 mM glycine-NMG pH$_o$ 9, plus variable concentrations of NaCl as indicated, and NMG-Cl, up to a total cation concentration of 105 mM.

(E) [Ca^{2+}] dependence of CHR1 photocurrent. I/V plot of photocurrent at different [Ca^{2+}]. The solutions contained 0.1 mM $MgCl_2$ and 5 mM glycine-NMG, pH$_o$ 9, plus variable $CaCl_2$ concentrations and NMG-Cl up to a total cation concentration of 105 mM.

Na^+ in Figure 3D. The K_m for Na^+ could not be determined as the conductance is far from saturation, even at 100 mM Na^+ (Figure 3D). The situation for K^+ is similar (discussed below). By contrast, Ca^{2+}-carried currents were small (Figures 3B and 3C), but the affinity of the channel for Ca^{2+} was relatively high, with a K_m value of ~16 mM at −100 mV (Figure 3E).

Kinetic Selectivity Analysis

Traditionally, the selectivity of ion transport is estimated by changes of the reversal voltage under various ionic conditions using Goldman's constant field voltage equation (Hille, 2001). This approach assumes independent movement of the different ion species, which is not valid for individual transporter molecules, where different substrates will compete for the available binding site(s). We applied a kinetic approach and used not only the reversal voltages but also the nonlinear current–voltage relationships for evaluating experimental data. One possible result of this analysis was to discern, using physiochemically sound means, whether binding or transport is the selective reaction step in the enzymatic transport cycle of CHR1. For this analysis, the reaction scheme in Figure 4A was used. Experimental data and fitted curves for K^+ relations are shown in Figure 4B. The good fits of experimental and calculated values render the approach realistic. The solution shown represents the best fit that was reached consistently with moderately varying start values and was therefore considered unambiguous. The fit confirms the assumed internal concentration of 120 mM cations (mostly K^+), besides H^+, which can pass through

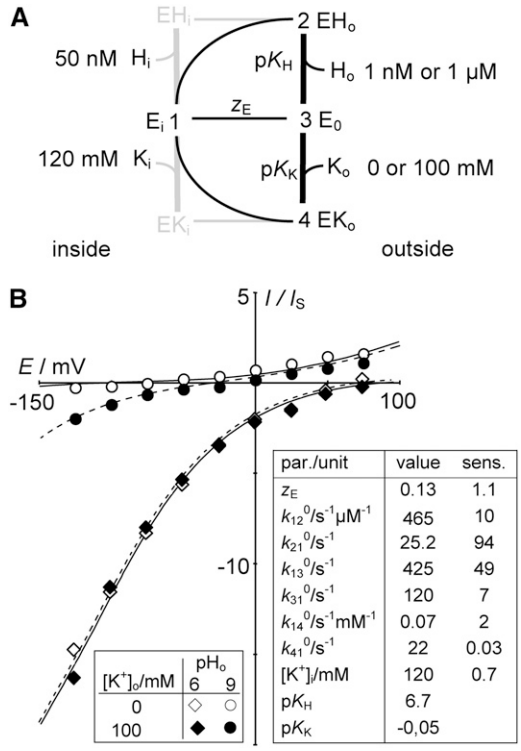

Figure 4. Kinetic Selectivity Analysis.

(A) Minimum reaction scheme and nomenclature for competitive translocation of H^+ and an alternate monovalent cation, here K^+, through an ion translocating enzyme (E) according to Gradmann et al. (1987). Voltage-sensitive and temporally resolved reactions between inside and outside can be determined explicitly by steady state current–voltage relationships recorded at different external concentrations of H^+ and K^+ and are represented by standard line width. Bold lines: $pK_H = \ln((1/K_2)$ and $pK_K = \ln((1/K_4)$ mark fast binding and debinding reactions outside with the equilibrium constants $K_2 = k_{32}/k_{23}$ and $K_4 = k_{34}/k_{43}$ for fast binding and debinding reactions outside, correspond to $pK_H = -\ln_{10}(1/K_2)$ and $pK_K = -\ln_{10}(1/K_4)$, respectively. z_E, apparent charge number of unoccupied binding site (Andersen, 1989). Gray, supplementation of reaction scheme by distinction of fast inner binding equilibria and slow translocation steps, which could be identified when inner concentrations of H^+ and K^+ were changed as well during experimentation (not done here).

(B) Example of analysis by fitting the independent parameters of the model in **(A)** to experimental steady state current–voltage relationships (points) in the presence and absence of 100 mM K^+ at pH_o 9 and pH_o 6. Inset table: numerical results of fit (value) and sensitivity (sens.); sensitivity is expressed as increase of mean SD in 0.1% upon ±10% deviations of the parameter from its fitted optimum value.

the CHR1 channel. This concentration is closely related to the observed reversal voltages. The numerical results listed in the inset of Figure 4B show not only the fitted parameter values but also sensitivity coefficients, which describe the numerical impact of the individual parameters for the fit quality. Parameters with small sensitivity coefficients (e.g., of $k_{41}{}^0$) are not critical for the shape of the current–voltage curves and have little statistically significant effect under the present configuration, whereas parameters with large sensitivity coefficients (e.g., of $k_{21}{}^0$) have a strong effect on the current–voltage curves and are highly significant.

If the apparently extreme values of the fundamental rate constants $k_{12}{}^0 \approx 465\ s^{-1}\mu M^{-1}$ and $k_{14}{}^0 \approx 0.07\ s^{-1}mM^{-1}$ are multiplied by the corresponding substrate concentrations of $[H^+]_i \approx 50$ nM and $[K^+]_i \approx 120$ mM, the apparent rate constants $k_{12} = k_{12}{}^0[H^+]_i \approx 23\ s^{-1}$ and $k_{12} = k_{12}{}^0[H^+]_i \approx 8.4\ s^{-1}$ are well within the same order of magnitude under physiological conditions. Likewise, k_{41} and k_{21} are similar for the two substrates, and the rate constants of reorientation of the empty binding site, k_{13}, and k_{31}, are shared by the two transport cycles. However, the binding equilibria pK_H and pK_K indicate a much stronger affinity of the binding site for the primary substrate H^+ compared with the alternate substrate K^+. These equilibria were not fitted as independent parameters; they rather are dictated thermodynamically by $pK_H = -\ln_{10}[k_{21}{}^0k_{13}{}^0/(k_{12}{}^0k_{31}{}^0)]$ and $pK_K = -\ln_{10}[k_{41}{}^0k_{13}{}^0/(k_{14}{}^0k_{31}{}^0)]$. In conclusion, by this analysis the selective step of the enzymatic transport cycle in CHR1 can be assigned to the binding equilibrium, whereas translocation seems to be equally efficient for both K^+ and H^+.

CHR1 Spectra

To provide evidence that CHR1 was indeed responsible for in vivo photocurrents and the behavior in the light, we aimed to compare the available action spectra with absorption spectra of purified CHR1. In an initial attempt to collect CHR1 protein, both a full-length CHR1-cDNA and a truncated version of the cDNA encoding $CHR1_{1\text{-}345}$ were expressed in *Escherichia coli* or in the methylotrophic yeast *Pichia pastoris*. In both cases, we were able to identify protein, but without functional chromophore. Finally, a CHR1 cDNA fragment encoding amino acids 1 to 357 (the portion of the protein that is relevant for ion channel activity) could be expressed in green monkey COS-1 cells and purified via immunoaffinity chromatography. The amount of purified protein was low but sufficient for recording absorption spectra in the visible range. Dark-adapted CHR1 at pH 8.0 showed an absorption spectrum with vibrational fine structure and a central maximum at around 463 nm (Figure 5A). Acidification of the medium to pH 4.5 shifted the maximum of the spectrum toward 505 nm with simultaneous loss of the spectral fine structure. These data indicate that $CHR1_{1\text{-}357}$ exists as two isoforms that are in pH-dependent equilibrium. The pK for the equilibrium was determined to be ~6.5. Both species are spectroscopically active and showed a red-shifted absorption in continuous 470-nm light (Figure 5B), but the photocycle could not be further analyzed using the small amount of purified protein available. To confirm the protochromism of the CHR1 absorption as an endogenous property of the native photoreceptor, photocurrent action spectra were recorded from CHR1-expressing oocytes at pH_o 9, 7.5, 6.5, and 5.5 at −75 mV (Figures 5C and 5D). At pH_o 9, the spectrum was centered at 470 nm with a half bandwidth of 95 nm. At pH_o 7.5, the spectrum became significantly broader and was at pH_o 6.5 shifted to a maximum of 495 nm, respectively. The pK for the transition is above 7.5, which is higher than the pK of the transition for the purified protein where the protein is at zero voltage and sensitive to the pH of the surrounding solution. However, the data show that the CHR1 absorption is also protochromic in a lipid environment.

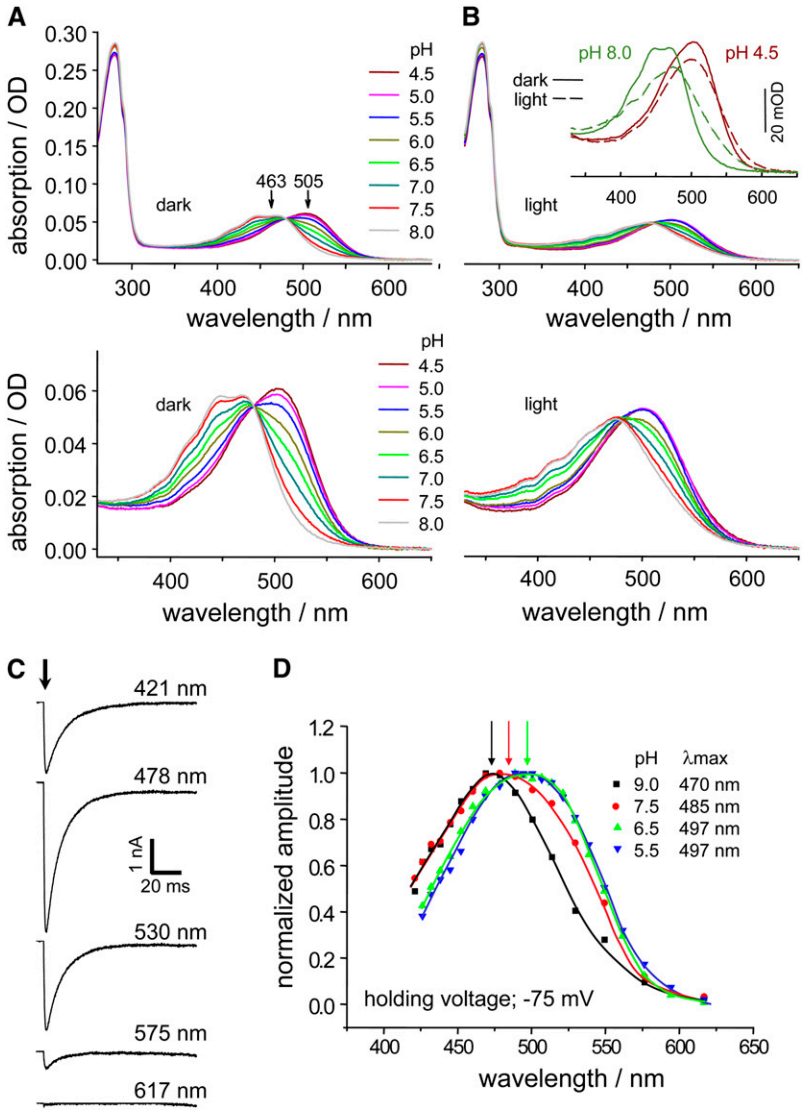

Figure 5. CHR1 Spectra.

(A) and **(B)** Spectra of purified dark-adapted CHR1 in dodecyl maltoside solution in darkness (**[A]**; dark) and upon permanent illumination with blue light from a 470-nm LED (**[B]**; light) at different pH values. Inset shows overlay of spectra at pH 4.5 and 8.0, respectively. Bottom panels are enlarged views of the top panels.

(C) Typical recording traces of CHR1 expressed in a *Xenopus* oocyte. CHR1 was excited with 10-ns laser flashes of various wavelengths (indicated by an arrow). The membrane voltage was clamped at –75 mV.

(D) Action spectra resulting from stimulation with laser flashes (as in **[B]**) at pH_o 9.0, 7.5, 6.5, and 5.5. Peak wavelengths are indicated by arrows. Data points are averages of 20 to 25 recordings. The current amplitudes were compared for equal photon irradiance (photons m^{-2}).

DISCUSSION

The experimental results presented here indicate that photocurrents of *Chlamydomonas* CW2 gametes are predominantly caused by CHR1, with only a small contribution by CHR2. No photocurrents can be detected when CHR1 is reduced, and, accordingly, neither photophobic responses nor phototaxis are observed. This correlation was expected because photocurrents trigger changes of the flagellar beat that provide the physical mechanism for phototaxis and photophobic responses (Holland et al., 1997) and is in line with the results of Sineshchekov et al. (2002) and Govorunova et al. (2004). In CW2 transformants containing variable amounts of CHR1, the strong correlation between photocurrent amplitude and CHR1 levels suggests that the residual amount of CHR2 in gametes of this strain does not significantly contribute to the photocurrents and, thus, to the behavioral response, whereas a significant contribution of CHR2 can be seen in vegetative cells especially after stimulation with 455-nm light. The conclusion that CHR1 is a multifunctional photoreceptor and alone able to mediate phototaxis

and photophobic responses was also demonstrated to be the case at alkaline pH.

In this study, we confirmed the earlier reported pH_o and voltage dependencies of CHR1 photocurrents (Nagel et al., 2002). Furthermore, we showed that CHR1 conducts significant amounts of Na^+, K^+, and Ca^{2+} between pH_o 6 and pH_o 9 (Figure 3). The relative conductance for alternate cations is similar to that of CHR2 (Nagel et al., 2003). However, the conductance of both channelrhodopsins is small for all cations except for protons, and both CHR1 and CHR2 are essentially proton channels. Considering that at pH_o 7 (10^{-7} M H^+) and 100 mM Na^+ (10^{-1} M Na^+), approximately half of the current is carried by H^+ and half by Na^+, the molar conductance for H^+ must be 10^6 times larger than that for Na^+ (at -120 mV), which corresponds well with the kinetically determined values of pK_H and pK_K in the numerical results of Figure 4B.

The transmembrane voltage of *Chlamydomonas* is assumed to rest, as in any typical plant cell, at an intermediate value between the more negative equilibrium voltage of a H^+ pump and the more positive value for electrodiffusion of ions. This means that the membrane voltage is higher (less negative) at more acidic pH (Malhotra and Glass, 1995) and that an increase in passive ion conductance will cause a depolarization under most circumstances. This is exactly what happens when CHR1 is illuminated, regardless of which cation species is available. Depolarization is generally accepted to be the common cause for all light-induced changes of flagellar motion in *Chlamydomonas* (Holland et al., 1997; Yoshimura and Kamiya, 2001). CHR1-like proteins might cause such light-induced depolarization in very different ecological environments, ranging from fresh water (low [Na^+] and high [H^+]) to sea water (high [Na^+] and low [H^+]) conditions.

To characterize CHR1, we obtained absorption spectra for purified CHR1, which showed a shift in the absorption maximum from 505 nm at pH 4.5 to 463 nm at pH 8.0. The action spectra from oocytes (Figure 5D) supported that CHR1 exists as two species distinguishable by their clearly separated absorption and action spectra maxima. These data confirmed earlier reported CHR1 action spectra recorded from oocytes at pH_o 5.5, showing a maximum at 495 nm (Nagel et al., 2003) compatible with the *Chlamydomonas* spectra. However, a discrepancy occurred in the sense that CHR1 action spectra peaked at 470 nm in an alkaline pH and at 495 nm under acidic conditions, whereas low intensity spectra for phototaxis and photophobic responses peak at 495 to 505 nm (Foster et al., 1984; Harz and Hegemann, 1991; Sineshchekov et al., 1994; Ehlenbeck et al., 2002). This might be explained by the pK for the transition between the two isoforms, which is near 6.5 in solubilized CHR1 and shifted to a higher pK_o (extracellular changes) above 7.5 in oocytes. One possible reason for the pK shift is that in oocytes the pH is changed extracellularly, whereas the main influence might result from the intracellular side (pH_i), which is only slightly influenced as a secondary effect in our oocyte experiments. Taking into account that most action spectra data were collected at pH_o 6 or 6.8, the in vivo results are quite compatible with the acidic form of CHR1 serving as the major photoreceptor.

High intensity phototaxis action spectra of many green algae exhibit, in addition to the maximum at 500 nm, a shoulder near 460 nm (Halldal, 1958; Nultsch et al., 1971). The activity at 460 nm was explained in the past by CHR2 (Sineshchekov et al., 2002), which indeed shows peak absorption and activity at 470 nm (Nagel et al., 2003; Bamann et al., 2008; Ernst et al., 2008). But now, CHR1 has also to be taken into account for behavioral responses to blue light ($\lambda < 480$ nm) and in particular when the responses are recorded at high pH_o. An important question that remains is in which respect CHR1 protochromism is advantageous for the living alga. It is conceivable that *Chlamydomonas* makes use of protochromism for switching between positive and negative phototaxis, depending on the pH_o of the medium or, more importantly, the internal pH_i as a result of photosynthetic activity.

METHODS

Cell Culture

For all experiments, the cell wall–deficient *Chlamydomonas reinhardtii* strain CW2 was used. Vegetative cells were grown in high salt acetate medium (HSA) under cool fluorescent white light (70 W/m^2, 25°C, 120 rpm) up to the early log phase ($OD_{800} = 0.2$ to 0.7; $2 \cdot 10^6$ to $7 \cdot 10^6$ cells/mL). Cells were differentiated into gametes overnight in nitrogen-free NMM medium (80 μM $MgSO_4$, 100 μM $CaCl_2$, 3.1 mM K_2HPO_4, and 3.4 mM KH_2PO4, pH 6.8). For all physiological studies, cells were transferred to 5 mM HEPES, 9 mM HCl, 0.1 mM KCl, 0.3 mM $CaCl_2$, and 10 μm BAPTA adjusted with NMG to pH 6.8 and adapted for 30 min under dim light (4 W/m^2).

Antibody Generation

Both channelrhodopsins, CHR1 and CHR2, are large 7-TM membrane proteins (of 76 to 77 kD) with large C-terminal extensions of unknown function. Since the 7-TM fragments were difficult to express in *Escherichia coli*, polyclonal antibodies were produced in rabbits against recombinant C-terminal fragments of CHR1 (amino acids 310 to 547) and CHR2 (amino acids 272 to 520) that were expressed as C-terminal fusions with maltose binding protein and affinity-purified using Amylose resin (New England Biolabs). Antibodies were affinity purified using recombinant C-terminal protein fragments of CHR1 (amino acids 310 to 712) and CHR2 (amino acids 272 to 737), containing a 6× histidine tag at the C terminus. Protein fragments were expressed in *E. coli* and affinity purified using Ni-NTA Superflow resin (Qiagen).

Immunoblot Analysis

Due to the rapid degradation of the CHR proteins during preparation of membrane fractions even at 4°C and in the presence of protease inhibitors, whole-cell extracts were used for immunoblot analysis. Cells were harvested by centrifugation, lysed directly in Laemmli sample buffer, and heated up to 95°C for 3 min. Proteins of 1.5×10^6 cells (for CHR1 detection) and 3×10^6 cells (for CHR2 detection) were separated on a 10% SDS gel (10 × 10 cm), transferred to nitrocellulose membranes by semidry blotting (2.5 mA/cm^2, 40 min), and incubated with primary antibodies overnight at room temperature (anti-CHR1, 1:5000; anti-CHR2, 1:3000 in PBS). Signals were visualized using secondary horseradish peroxidase–labeled antibodies together with the ECL system from Amersham on x-ray films. A clear distinction between CHR1 and CHR2 was possible under nonreducing electrophoresis conditions (without β-mercaptoethanol in the sample buffer) where CHR1 appeared as a dimer at 140 kD. For quantification, films were scanned and analyzed with the software Optiquant (Packard Instruments).

Construction of the RNAi Plasmid and Transformation

The *pPB-ASCHR1* RNAi plasmid was constructed by sequentially inserting *HSP70A-rbcS2* promoter (Schroda et al., 2000) between *Sac*I and *Xho*I, CHR1 genomic cDNA fragment (1538 to 3186 bp) between *Xho*I and *Bam*HI, CHR1 cDNA fragment (472 to 975 bp) in reverse orientation between *Bam*HI and *Kpn*I, and the hygromycin selection marker (aph7′) (Berthold et al., 2002) into the *Nae*I site of pBluescript II SK+ (Stratagene). The cell wall–deficient strain CW2 was transformed with the pPB-ASCHR1 plasmid using the glass bead method from Kindle (1990). Oligonucleotides used as PCR primers are listed in Supplemental Table 1 online.

Indirect Immunofluorescence

Indirect immunofluorescence was performed on both vegetative cells and gametes of *C. reinhardtii* wild-type strain CC124, cell wall–deficient strain CC851 (*cw2 mt+*), and the *cw2*-derived RNAi strain H17 according to the method of Johnson and Rosenbaum (1992), with several modifications. Vegetative cells grown in TAP (CC124) or HSA (CC851, H17) medium to a density of 3 to 8 $\times$ 10^6 cells/mL were harvested and resuspended to $\sim$$10^7$ cells/mL in TAP medium containing autolysin (for removal of cell walls; CC124) or in HSA (CC851, H17). Gametes were induced in NMM medium, harvested, and resuspended at a cell density of 5 $\times$ 10^6 to 10^7 cells/mL in NMM (CC851, H17) or NMM that contained autolysin for strain CC124. For regrowth of flagella, cell suspensions were incubated for 1 h at room temperature with gentle stirring. Then an equal volume of microtubule stabilizing buffer (MTSB; 30 mM PIPES, pH 6.8, 25 mM KCl, 5 mM $MgSO_4 \cdot 7H_2O$, and 5 mM EGTA) containing 10% hexylene glycol (MTSB/HG) was added dropwise. Aliquots of 250 μL cell suspension were transferred to cover slips pretreated with poly-L-lysine for efficient cell adhesion. After 15 min, the supernatant was removed and immediately replaced by an equal volume of MTSB/HG. Following the same routine, fixation solution (73.5% MTSB/HG, 4% paraformaldehyde, and 0.3% Nonidet P-40) was added followed by a 45-min incubation period. Cover slips were washed in PBS/0.05% Tween 20 four times and then blocked in PBS containing 0.05% Tween 20 supplemented with 1% BSA for 30 min. Primary antibodies were diluted in blocking buffer 1:250 (monoclonal anti α-tubulin antibody B-5-1-2; Sigma-Aldrich) or 1:100 (anti-CHR1 antibody CHR1-2), respectively, and added to the cover slips, followed by an overnight incubation at 4°C. After four successive washes in PBS/0.05% Tween 20, Alexa-Fluor 488–conjugated goat anti-mouse IgG (Molecular Probes) diluted 1:1000 in PBS was used as a secondary antibody against tubulin-specific primary antibody B-5-1-2, and Alexa-Fluor 546–conjugated goat anti-rabbit IgG (Molecular Probes) diluted 1:1000 in PBS was used as a secondary antibody against channelrhodopsin-specific antibody anti-CHR1. After 2 h of incubation at room temperature in the dark, the secondary antibodies were removed, the samples washed four times in PBS/0.05% Tween 20, and cover slips were mounted with a 15-μL drop mounting medium (GLOW mounting medium; ENERGENE). Samples were inspected using a Zeiss LSM510-Meta confocal laser scanning microscope equipped with a $\times$100 PlanApochromat objective (numerical aperture 1.4). Fluorescence signals of Alexa-Fluor 488 (excitation 488 nm, argon laser) were detected using a 505- to 550-nm band-pass filter and of Alexa-Fluor 546 (excitation 543 nm, HeNe laser) using a 560-nm long-pass filter. Sequential scanning (using the multitrack mode) was performed to avoid any crosstalk of fluorescence channels.

Light Scattering

Phototactic orientation was measured using a multiangle light-scattering apparatus (Schaller et al., 1997), which allowed orientation changes of a *Chlamydomonas* population to be determined upon stimulation with monochromatic light with high time resolution. In brief, parallelized infrared light was scattered by a *Chlamydomonas* suspension ($1 \cdot 10^6$/mL) in a fluorescence cuvette (20 $\times$ 10 mm, SOG 3; Starna) onto infrared sensitive photodiodes that were orientated at a scattering angle of 14° in a clockwise manner. The intensity of the scattered light (i.e., the current produced by the IR diode corresponding to the 9 o'clock position) was passed through a current voltage amplifier (10^6 V/A) and a 10-Hz low-pass filter using the signal conditioner CyberAmp 320 (Molecular Devices). The voltage proportional to the intensity of the scattered light was recorded and analyzed using the data acquisition system Digidata 1322A together with the software pClamp9 (Molecular Devices). As stimulating light source, LuxeonStar-LEDs (Quadica Developments) with the wavelengths 450, 505, and 530 nm were used. Light intensities were adjusted using neutral-density filters (AHF Analysentechnik).

Dish Test/Phototaxis

As a simple assay for determining the phototactic rate of *Chlamydomonas* cells, the dish test was used (Hegemann et al., 1988). Cell suspensions with a density of 1 $\times$ 10^7 cells per mL were poured into a small Petri dish (diameter of 3.5 cm) and illuminated from one side with white light (7 W/m^2). The migration of the cells away from the light source was observed for 6 min.

Photophobic Responses

Photophobic responses were analyzed by recording the swimming speed of individual cells, using a dark-field microscope (Zeiss Axiovert 100) with $\times$5 objective and the real-time motion analysis software WinTrack 2000XP (Real Time Computers). The cells were inserted into a fluorescence cuvette (d = 2 mm; Starna 28F) at a cell density of 0.5 to $1 \cdot 10^6$/mL. Infrared light was used to visualize the cells on a monitor. The program settings where selected such that $\sim$120 cells were tracked simultaneously. Flashes of green light (505 $\pm$ 40 nm, $4 \cdot 10^{22}$ photons/m^2) were used to evoke photophobic responses that were analyzed using the LongTrackModule option of the program.

Heterologous Expression in *Xenopus laevis* Oocytes

A full-length cRNA, $CHR1_{1\text{-}712}$ (amino acids 1 to 712), and a truncated version, $CHR1_{1\text{-}346}$ (amino acids 1 to 346), were synthesized in vitro from NheI-linearized pGEMHE-plasmid using T7 RNA polymerase (mMessage mMachine; Ambion) (Nagel et al., 2002). Because the transport properties of both were qualitatively indistinguishable, most experiments were performed with $CHR1_{1\text{-}346}$. Oocytes from female Xenopus (Ecocyte Bioscience) were injected with 50 nL CHR1-cRNA (0.5 to 1 μg/μL) and incubated in the dark at 18°C in Ringers solution (96 mM NaCl, 2 mM KCl, 1.8 mM CaCl2, 1 mM MgCl2, and 5 mM MOPS-NaOH, pH 7.5) in the presence of 5 mM Na-pyruvate, 50 μg/mL gentamicin, and 1 μM all-trans-retinal (Sigma-Aldrich).

Electrophysiology

Electrophysiological measurements on *Chlamydomonas* were done in principle as described previously (Harz and Hegemann, 1991; Ehlenbeck et al., 2002), with some modifications. Briefly, pipettes for recording photocurrents directly from the eyespot were pulled from borosilicate glass capillaries (1.8 mm, 0.15-mm walls, Kimax-51; Witz Scientific) in two steps and polished until the tip diameter reached 1.5 μm. The cone angle was $\sim$30°. The pipettes were filled with NMG^+/K^+ buffer (5 mM HEPES, 9 mM HCl, 0.1 mM KCl, and 10 μM BAPTA, adjusted with NMG to pH 6.8 or 9.0) containing 0.2 mM $CaCl_2$. Before measurements, cells were incubated in the NMG^+/K^+ buffer for 20 min under dim light (4 W/m^2). The resistance of the pipette was 20 to 40 MΩ and reached

120 to 160 MΩ when the region of the cell containing the eye was sucked into the pipette. A ×40 objective and a ×4 phototube were used for identifying the eyespot by infrared light on a monitor. Cells were stimulated with green light pulses (500 ± 40 nm) of 300-ms duration and an intensity of 4×10^{22} photons $m^{-2}s^{-1}$. Measurements were performed at room temperature (20°C). Data were recorded using the data acquisition system Digidata 1322A and analyzed with the software pClamp (Molecular Devices).

Two-electrode voltage clamp measurements were performed on *Xenopus* oocytes using a GeneClamp 500 amplifier (Axon Instruments) and a Turbo Tec-05X (NPI Electronic). Data acquisition and light triggering were controlled with pCLAMP software via DigiData 1322A or 1440A interfaces (Molecular Devices). The microelectrodes were fabricated by pulling borosilicate glass capillaries (1.5-mm o.d. and 1.17-mm i.d.) using a micropipette puller (model P-97; Sutter Instruments) and filled with 3 M KCl. The resistance of microelectrodes was 0.5 to 1.5 MΩ. A 75-W Xenon lamp (Jena Instruments) was used for the source of light pulse. The light was passed through a K50 filter (Balzers) and applied to the oocytes using a light guide (diameter of 2 mm). The light intensity was 1.5×10^{22} photons s^{-1} m^{-2} at the surface of the oocyte. The data obtained were averages of more than three experiments.

Action spectra were recorded using tunable 10-ns laser flashes as described by Ernst et al. (2008).The amplifier Tec-05X was compensated in such a way that the voltage change was kept below 0.05 mV at a half saturating laser flash. Data were recorded at high gain with a sampling rate of 250 kHz. The laser intensity varied from flash to flash within a range of 5%. The data were averages of 10 to 30 recordings. The solution contained 100 mM NaCl, 1 mM $MgCl_2$, and 0.1 mM $CaCl_2$, with 5 mM glycine, pH 9.0, 5 mM MOPS, pH 7.5 and 6.5, or 5 mM citrate, pH 5.5. In experiments with high extracellular Ca^{2+}, prior to measurements, 10 mM BAPTA was injected into the oocyte to inhibit endogenous Ca^{2+}-sensitive chloride channels.

CHR1 Expression in COS-1 Cells

For expression in COS-1 cells (ATCC, CRL-1650), a CHR1 encoding cDNA fragment corresponding to amino acids 1 to 357 plus a nucleotide sequence corresponding to the C-terminal TETSQVAPA sequence (1D4-epitope) (Molday and Mackenzie, 1983) was amplified by PCR and inserted between the *Eco*RI-*Not*I sites of the expression vector pMT3 to replace the opsin gene (Franke et al., 1988; Khorana, 1993). Tissue culture, transient transfection with the resulting CHR1-pMT3 vector followed by further incubation in the presence of 3 μM all-*trans*-retinal, cell harvest 3 d after transfection, and purification of CHR1 was performed as described for bovine rhodopsin (Franke et al., 1988; Meyer et al., 2000; Fritze et al., 2003). CHR1 was solubilized with dodecyl maltoside and purified by immunoaffinity adsorption using the rho 1D4 antibody coupled to CNBr-activated Sepharose 4 Fast Flow (GE Healthcare). CHR1 was eluted with 100 μM of an 18-mer peptide corresponding to the C-terminal rhodopsin sequence in 0.03% (w/v) dodecyl maltoside and 5 mM 1,3-bis[tris(hydroxymethyl)methylamino propane, pH 6.0 (Meyer et al., 2000; Fritze et al., 2003). Eluates were concentrated using centricon YM-10 (Millipore) concentrators. The mouse antirhodopsin monoclonal antibody rho 1D4 used for purification of CHR1 was purchased from the University of British Columbia (R. Molday).

Spectroscopy

For absorption spectroscopy at 20°C, a Cary 50 Bio spectrophotometer (Varian) with a spectral resolution of 1 nm was used. Spectra of CHR1 were taken in the dark (dark-adapted CHR1) or under continuous illumination, perpendicular to the measuring beam applied by a blue Luxeon LED (470 nm; Philips Lumileds). pH was adjusted by addition of one-third volume buffer solution yielding final concentrations of 20 mM citrate, pH 4 to 6.5, 20 mM MOPS, pH 7 and 7.5, or 20 mM Tris, pH 8 and 8.5, plus 100 mM NaCl, 0.1 mM $CaCl_2$, and 0.1 mM $MgCl_2$.

Numerical Analysis

For fits, a least square alogorithm was used, repeating small parameter changes by common increments (e.g., ±0.1%) simultaneously, as described before (Allen et al., 1998). The results of Figure 4B were obtained with the following strategy. (for definitions see Figure 4A). First, the five parameters (z_E, k_{12}^0, k_{21}^0, k_{13}^0, and k_{31}^0) of the H^+ loop were determined from data at different pH_o and $[K^+]_o = 0$; second, k_{14}^0 and k_{41}^0 of the K^+ loop could be determined in addition with experiments at $[K^+]_o = 100$ mM. Superscript 0 marks reference conditions, [i.e., zero voltage and reference concentration as marked. In the third and final step, all eight independent parameters (z_E, the six k^0 values, and the internal concentration of conducted cations besides H^+) were fitted simultaneously (continuous curves) using the available estimates as start values. Notes: the fundamental equilibrium constants K_2^0 and K_4^0 are not independent parameters but $K_2^0 = k_{21}^0 k_{13}^0/(k_{31}^0 k_{12}^0)$ and $K_4^0 = k_{41}^0 k_{13}^0/(k_{31}^0 k_{14}^0)$; voltage enters the system by voltage sensitive rate constants [e.g., $k_{13} = k_{13}^0 \exp(z_E u/2)$ and $k_{31} = k_{31}^0 \exp(-z_E u/2)$], where $u = EF/(RT)$ is the reduced transmembrane voltage, and the factor 1/2 in the exponent reflects the assumption of a corresponding symmetrical Eyring barrier.

Accession Numbers

Sequence data from this article can be found in the GenBank/EMBL data libraries under the following accession numbers: AF385748, CHR1 encoding mRNA and protein sequence; AF508967, CHR1 encoding genomic sequence, annotated as *COP3* in the *Chlamydomonas* genome (NW_001843888).

Supplemental Data

The following materials are available in the online version of this article.

Supplement Figure 1. Specificity of the Anti-CHR Antibodies and Expression of the CHRs in the Strain CW2.

Supplement Figure 2. Editing of *CHR1* RNA.

Supplement Table 1. Oligonucleotides Used for Plasmid Construction.

ACKNOWLEDGMENTS

We thank Helena Seibel, Jana Engelmann, Anja Koch, and Maila Reh for technical assistance, Pedro Sánchez Murcia for cloning of CHR1-pMT3, Werner Müller-Esterl for providing a CHR1-loop1/2–specific monoclonal antibody, and Telsa Mittelmeier for critical reading of the manuscript and discussion. The work was supported by the Deutsche Forschungsgemeinschaft Sfb498 and HE1535/13-3 (P.H.), and Sfb449 and Sfb740 (O.P.E.).

Received January 2, 2008; revised April 25, 2008; accepted May 24, 2008; published June 13, 2008.

REFERENCES

Allen, G.J., Sanders, D., and Gradmann, D. (1998). Calcium-potassium selectivity: Kinetic analysis of current-voltage relationships of the open, slowly activating channel in the vacuolar membrane of guard-cells of *Vicia faba.* Planta **204:** 528–541.

Andersen, O.S. (1989). Kinetics of ion movement mediated by carriers and channels. Methods Enzymol. **171:** 62–112.

Bamann, C., Kirsch, T., Nagel, G., and Bamberg, E. (2008). Spectral characteristics of the photocycle of channelrhodopsin-2 and its implication for chennel function. J. Mol. Biol. **375:** 686–694.

Beckmann, M., and Hegemann, P. (1991). In vitro identification of rhodopsin in the green alga *Chlamydomonas.* Biochemistry **30:** 3692–3697.

Berthold, P., Schmitt, R., and Mages, W. (2002). An engineered *Streptomyces hygroscopicus* aph 7" gene mediates dominant resistance against hygromycin B in *Chlamydomonas reinhardtii.* Protist **153:** 401–412.

Bi, A.D., Cui, J.J., Ma, Y.P., Olshevskaya, E., Pu, M.L., Dizhoor, A.M., and Pan, Z.H. (2006). Ectopic expression of a microbial-type rhodopsin restores visual responses in mice with photoreceptor degeneration. Neuron **50:** 23–33.

Boyden, E.S., Zhang, F., Bamberg, E., Nagel, G., and Deisseroth, K. (2005). Millisecond-timescale, genetically targeted optical control of neural activity. Nat. Neurosci. **8:** 1263–1268.

Ehlenbeck, S., Gradmann, D., Braun, F.J., and Hegemann, P. (2002). Evidence for a light-induced H^+ conductance in the eye of the green alga *Chlamydomonas reinhardtii.* Biophys. J. **82:** 740–751.

Ernst, O., Sanchez Murcia, P.A., Daldrop, P., Tsunoda, S.P., Kateriya, S., and Hegemann, P. (2008). Photoactivation of channelrhodopsin. J. Biol. Chem. **283:** 1637–1643.

Foster, K.W., Saranak, J., Patel, N., Zarilli, G., Okabe, M., Kline, T., and Nakanishi, K. (1984). A rhodopsin is the functional photoreceptor for phototaxis in the unicellular eukaryote Chlamydomonas. Nature **311:** 756–759.

Franke, R.R., Sakmar, T.P., Oprian, D.D., and Khorana, H.G. (1988). A single amino-acid substitution in rhodopsin (lysine 248—leucine) prevents activation of transducin. J. Biol. Chem. **263:** 2119–2122.

Fritze, O., Filipek, S., Kuksa, V., Palczewski, K., Hofmann, K.P., and Ernst, O.P. (2003). Role of the conserved NPxxY(x)(5,6)F motif in the rhodopsin ground state and during activation. Proc. Natl. Acad. Sci. USA **100:** 2290–2295.

Govorunova, E.G., Jung, K.H., Sineshchekov, O.A., and Spudich, J.L. (2004). Chlamydomonas sensory rhodopsin A and B: Cellular content and role in photophobic response. Biophys. J. **86:** 2342–2349.

Gradmann, D., Klieber, H.G., and Hansen, U.P. (1987). Reaction kinetic parameters for ion transport from steady-state current voltage curves. Biophys. J. **51:** 569–585.

Halldal, P. (1958). Action spectra of phototaxis and related problems in Volvocales, Ulva Gametes and Dinophyceae. Physiol. Plant. **11:** 118–153.

Harz, H., and Hegemann, P. (1991). Rhodopsin-regulated calcium currents in *Chlamydomonas.* Nature **351:** 489–491.

Hegemann, P. (2008). Algal sensory photoreceptors. Annu. Rev. Plant Biol. **59:** 167–189.

Hegemann, P., and Bruck, B. (1989). The light induced stop response in *Chlamydomonas reinhardtii.* Cell Motil. **14:** 501–515.

Hegemann, P., Fuhrmann, M., and Kateriya, S. (2001). Algal sensory photoreceptors. J. Phycol. **37:** 668–676.

Hegemann, P., Hegemann, U., and Foster, K.W. (1988). Reversible bleaching of *Chlamydomonas reinhardtii* rhodopsin in vivo. Photochem. Photobiol. **48:** 123–128.

Hegemann, P., and Uhl, R. (1990). Visual transduction in plant cells: Optical recording of rhodopsin-regulated intracellular processes from Chlamydomonas. Biophys. J. **57:** A217–A217.

Hille, B. (2001). Ion Channels of Excitable Membranes. (Sunderland, MA: Sinauer Associates).

Holland, E.M., Braun, F.J., Nonnengasser, C., Harz, H., and Hegemann, P. (1996). Nature of rhodopsin-triggered photocurrents in Chlamydomonas. 1. Kinetics and influence of divalent ions. Biophys. J. **70:** 924–931.

Holland, E.M., Harz, H., Uhl, R., and Hegemann, P. (1997). Control of phobic behavioral responses by rhodopsin-induced photocurrents in Chlamydomonas. Biophys. J. **73:** 1395–1401.

Ishizuka, T., Kakuda, M., Araki, R., and Yawo, H. (2006). Kinetic evaluation of photosensitivity in genetically engineered neurons expressing green algae light-gated channels. Neurosci. Res. **54:** 85–94.

Johnson, K.A., and Rosenbaum, J.L. (1992). Polarity of flagellar assembly in Chlamydomonas. J. Cell Biol. **119:** 1605–1611.

Jung, K. (2007). The distinct signaling mechanisms of microbial sensory rhodopsins in archaea, eubacteria and eukarya. Photochem. Photobiol. **83:** 63–69.

Kateriya, S., Nagel, G., Barnberg, E., and Hegemann, P. (2004). ''Vision'' in single-celled algae. News Physiol. Sci. **19:** 133–137.

Khorana, H.G. (1993). Two light-transducing membrane proteins: Bacteriorhodopsin and the mammalian rhodopsin. Proc. Natl. Acad. Sci. USA **90:** 1166–1171.

Kindle, K.L. (1990). High-frequency nuclear transformation of *Chlamydomonas reinhardtii.* Proc. Natl. Acad. Sci. USA **87:** 1228–1232.

Li, X., Gutierrez, D.V., Hanson, M.G., Han, J., Mark, M.D., Chiel, H., Hegemann, P., Landmesser, L.T., and Herlitze, S. (2005). Fast noninvasive activation and inhibition of neural and network activity by vertebrate rhodopin and green algae channelrhodopsin. Proc. Natl. Acad. Sci. USA **102:** 17816–17821.

Litvin, F.F., Sineshchekov, O.A., and Sineshchekov, V.A. (1978). Photoreceptor electric-potential in phototaxis of alga *Haematococcus pluvialis.* Nature **271:** 476–478.

Mahendran, R., Spottswood, M.R., and Miller, D.L. (1991). RNA editing by cytidine insertion in mitochondria of *Physarum polycephalum.* Nature **349:** 434–438.

Malhotra, B., and Glass, A.D.M. (1995). Potassium fluxes in *Chlamydomonas reinhardtii* (I. Kinetics and electrical potentials). Plant Physiol. **108:** 1527–1536.

Meyer, C.K., Bohme, M., Ockenfels, A., Gärtner, W., Hofmann, K.P., and Ernst, O.P. (2000). Signaling states of rhodopsin - Retinal provides a scaffold for activating proton transfer switches. J. Biol. Chem. **275:** 19713–19718.

Molday, R.S., and Mackenzie, D. (1983). Monoclonal antibodies to rhodopsin: Characterization, cross-reactivity, and application as structural probes. Biochemistry **22:** 653–660.

Nagel, G., Brauner, M., Liewald, J.F., Adeishvili, N., Bamberg, E., and Gottschalk, A. (2005). Light activation of channelrhodopsin-2 in excitable cells of *Caenorhabditis elegans* triggers rapid behavioral responses. Curr. Biol. **15:** 2279–2284.

Nagel, G., Ollig, D., Fuhrmann, M., Kateriya, S., Mustl, A.M., Bamberg, E., and Hegemann, P. (2002). Channelrhodopsin-1: A light-gated proton channel in green algae. Science **296:** 2395–2398.

Nagel, G., Szellas, T., Huhn, W., Kateriya, S., Adeishvili, N., Berthold, P., Ollig, D., Hegemann, P., and Bamberg, E. (2003). Channelrhodopsin-2, a directly light-gated cation-selective membrane channel. Proc. Natl. Acad. Sci. USA **100:** 13940–13945.

Nonnengasser, C., Holland, E.M., Harz, H., and Hegemann, P. (1996). The nature of rhodopsin-triggered photocurrents in Chlamydomonas. 2. Influence of monovalent ions. Biophys. J. **70:** 932–938.

Nultsch, W., Throm, G., and Rimscha, I.V. (1971). Phototactic investigations in *Chlamydomonas reinhardii* Dangeard in homocontinuous culture. Arch. Mikrobiol. **80:** 351–369.

Schaller, K., David, R., and Uhl, R. (1997). How Chlamydomonas keeps track of the light once it has reached the right phototactic orientation. Biophys. J. **73:** 1562–1572.

Schmidt, M., et al. (2006). Proteomic analysis of the eyespot of *Chlamydomonas reinhardtii* provides novel insights into its components and tactic movements. Plant Cell **18:** 1908–1930.

Schroda, M., Blocker, D., and Beck, C.F. (2000). The HSP70A

promoter as a tool for the improved expression of transgenes in Chlamydomonas. Plant J. **21:** 121–131.

Schroll, C., Riemensperger, T., Bucher, D., Ehmer, J., Voller, T., Erbguth, K., Gerber, B., Hendel, T., Nagel, G., Buchner, E., and Fiala, A. (2006). Light-induced activation of distinct modulatory neurons triggers appetitive or aversive learning in Drosophila larvae. Curr. Biol. **16:** 1741–1747.

Sharma, A.K., Spudich, J.L., and Doolittle, W.F. (2006). Microbial rhodopsins: Functional versatility and genetic mobility. Trends Microbiol. **14:** 463–469.

Simpson, L., Aphasizhev, R., Gao, G., and Kang, X. (2004). Mitochondrial proteins and complexes in Leishmania and Trypanosoma involved in U-insertion/deletion RNA editing. RNA **10:** 159–170.

Sineshchekov, O.A., Govorunova, E., Der, A., Keszthelyi, L., and Nultsch, W. (1994). Photoinduced electric currents in carotenoid-deficient Chlamydomonas mutants reconstituted with retinal and its analogs. Biophys. J. **66:** 2073–2084.

Sineshchekov, O.A., Jung, K.H., and Spudich, J.L. (2002). Two rhodopsins mediate phototaxis to low- and high-intensity light in *Chlamydomonas reinhardtii.* Proc. Natl. Acad. Sci. USA **99:** 8689–8694.

Sineshchekov, O.A., and Spudich, J.L. (2005). Sensory rhodopsin signaling in green flagellate algae. In Handbook of Photosensory Receptors, W.R. Briggs and J.L. Spudich, eds (Weinheim, Germany: Wiley-VCH Verlag), pp. 25–42.

Spudich, J.L. (2006). The multitalented microbial sensory rhodopsins. Trends Microbiol. **14:** 480–487.

Suzuki, T., et al. (2003). Archaeal-type rhodopsins in Chlamydomonas: Model structure and intracellular localization. Biochem. Biophys. Res. Commun. **301:** 711–717.

Uhl, R., and Hegemann, P. (1990). Probing visual transduction in a plant cell: Optical recording of rhodopsin-induced structural changes from *Chlamydomonas reinhardtii.* Biophys. J. **58:** 1295–1302.

Yoshimura, K., and Kamiya, R. (2001). The sensitivity of Chlamydomonas photoreceptor is optimized for the frequency of cell body rotation. Plant Cell Physiol. **42:** 665–672.

Zhang, F., Wang, L.P., Boyden, E.S., and Deisseroth, K. (2006). Channelrhodopsin-2 and optical control of excitable cells. Nat. Methods **3:** 785–792.

Zhang, Y.-P., and Oertner, T.G. (2007). Optical induction of synaptic plasticity using a light-sensitive channel. Nat. Methods **4:** 139–141.